River Flow 2006 – Ferreira, Alves, Leal & Cardoso (eds)
© 2006 Taylor & Francis Group, London, ISBN 0-415-40815-6

Discontinuities in geomorphic dam-break flows

Rui M.L. Ferreira & Sílvia Amaral
Instituto Superior Técnico, Lisbon, Portugal

João G.B. Leal
Universidade da Beira Interior, Covilhã, Portugal

Benoit Spinewine
Université catholique de Louvaine-la-Neuve, Louvaine-la-Neuve, Belgium

ABSTRACT: Geomorphic dam-break flows have been shown to feature discontinuities other than the downstream progressing wavefront. Of particular importance is the jump that forms, for some combinations of initial conditions and bed materials, near the location of the dam. No attempts to characterize this jump were undertaken until recently. In this text, the discontinuities occurring in geomorphic dam-break flows are investigated in the framework of a shallow-flow theory. The main objective is to understand whether they are susceptible to be described by Riemann waves or if they are flow features aroused by momentum sources, namely friction, or by phenomena beyond the shallow-flow theory. For that purpose, experimental results are presented and compared with a theoretical solution of the governing equations given initial discontinuous data. The classification of the discontinuities follows the comparison between the observed and calculated flow features for the same initial conditions. No attempt is made to address the phenomenological aspects of the formation and evolution of the discontinuities. Nevertheless, the observed behavior is discussed in conjunction with the weak solution of the governing equations.

1 INTRODUCTION

Geomorphic dam-break flows arise from the rapid release of stored water into a mobile bed channel and provoke important morphological changes in the downstream valley. Such flows propagate in the form of a bore, a type of wavefront, often laden with sediment, which, given the involved length scales, can be considered a discontinuity. The speed of this discontinuity, along with the maximum water depth associated to the dam-break flow, have been studied at length, as they constitute important elements for downstream risk assessment (Zech et al. 2004).

The wavefront may not be the only discontinuity in geomorphic dam-break flows. A hydraulic jump occurring near the location of the dam was reported in the early mobile-bed experiments of Chen and Simons (1979). More recently, Capart and Young (1998) drew attention to an upstream-progressing jump seen to form at early times at the dam location. For some combinations of initial conditions and bed material, the experimental results of Leal et al. (2002) also exhibit discontinuities forming at the vicinity of the dam and traveling at much smaller velocities than the wavefront. The experiments performed in these works do not provide a coherent body of data, since the shape and the dimensions of the flumes are too distinct to make the results commensurable. On safe grounds, only one observational result can be uttered: on prismatic rectangular mobile-bed channels, geomorphic dam-break flows resulting from the instantaneous removal of a vertical dam exhibit, for some combinations of initial conditions and bed material, a jump that forms near the location of the dam at early times and whose velocity is slower than that of the wave-front. This discontinuity will be henceforth called a *2-jump*.

The characterization of the wavefront benefits from more than one hundred years of theoretical and experimental studies (for the review of early results, *cf.* Stoker 1958, pp. 22–22). Quite on the contrary, the amount of empirical results concerning the 2-jump is virtually limited to the works cited in the preceding paragraph and the theoretical results are almost inexistent (see Ferreira 2005, pp. 303–305, for a review).

In this text, the discontinuities occurring in geomorphic dam-break flows are investigated. Special emphasis is placed on the quantification of the variables that

describe the 2-jump. It should be made clear that the thorough phenomenological characterization of these discontinuities will not be attempted. The main objective is to understand whether they are susceptible to be described by Riemann waves of the weak solution of the homogeneous part of the governing shallow-water equations or if they are flow features whose mathematical description requires a different formal treatment.

Empirical evidence, the experimental results described in Amaral (2004), §5, and Spinewine (2005) is compared with the solution of the governing equations, as presented by Ferreira (2005), pp. 396–430. The classification of the discontinuities follows the comparison between observed and calculated flow features for the same initial conditions. If the solution of the homogeneous shallow-water equations does not seem to describe occurring flow discontinuities, it is concluded that phenomena not included in the inertial and flux terms of the governing one-dimensional equations is responsible for the 2-jump.

The above methodology requires previous acquaintance with the conceptual model for the description of the geomorphic dam-break flows. It also requires some knowledge on the weak solution of the shallowwater equations given the dam-break Riemann problem. Both are addressed in the second section of the text. The third section is dedicated to the presentation of the experimental procedures and results. A comparison between the observed flow profiles and theoretical solution is carried out in the fourth section. The nature of the discontinuities is discussed in the fifth section. Finally, the text is ended by a number of concluding remarks.

2 CONCEPTUAL MODEL AND THEORETICAL SOLUTION

Written in vector notation, the first order, nonhomogeneous, hyperbolic system of conservation laws that describe geomorphic dam-break flows is

$$\partial_t \left(\mathbf{V} \left(\mathbf{U} \right) \right) + \partial_x \left(\mathbf{F} \left(\mathbf{U} \right) \right) = \mathbf{G} \left(\mathbf{U} \right) \tag{1}$$

where $\mathbf{V}$: $\mathbb{R} \times]0, +\infty[\rightarrow \mathbb{R}^3$ is the vector of dependent primitive variables, $\mathbf{U}$: $\mathbb{R}^3 \rightarrow \mathbb{R}^3$ is the vector of conservative variables, $\mathbf{F}$: $\mathbb{R}^3 \rightarrow \mathbb{R}^3$ is the flux vector, $\mathbf{G}$: $\mathbb{R}^3 \rightarrow \mathbb{R}^3$ is the vector of the source terms and x and t are the space and time co-ordinates, respectively.

Should the collapse of a dam be idealized as an instantaneous removal of a vertical barrier initially separating two constant states that extend indefinitely on both up- and downstream directions, as seen in figure 1, the mathematical expression of the dambreak problem is a Riemann problem. The conceptual model employed in this study to describe geomorphic dam-break flows is that developed by Ferreira 2005, §3. It

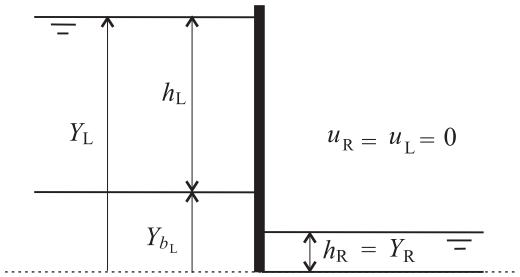

Figure 1. Initial conditions of the dam-break problem. The involved variables are: Y, the water elevation, h the water depth, Y_b the bed elevation and u, the depth-averaged flow velocity. The subscripts L and R stand for the initial left and right states, respectively.

features unsteady flow hydro- and sediment dynamics and channel morphology. In what concerns sediment dynamics, the dense limit approximation of the granular flow theory, rooted in Enskog's kinetic theory of dense gases (Chapman and Cowling 1970, §16), provided the theoretical background for the core of the model.

The one-dimensional conceptual model results from the integration of two-dimensional governing equations in an idealized layered domain. Multiple-layer shallow-water models were introduced by Capart (2000) and further developed by Fraccarollo and Capart (2002) and Spinewine (2005). Ferreira et al. (2003) followed a different approach. They considered that the total shear and normal stresses are continuous across the flow depth and into the bed and that the layers are mathematical idealizations based on the predominant type of stress.

Thus, the conceptual model employed in this study features i) a lowermost layer, the bed, composed of grains with no appreciable vertical or horizontal mean motion, ii) the contact load layer, where collisional stresses are dominant and iii) the suspended sediment layer, where turbulent stresses dominate (details in Ferreira 2005, pp. 229–231).

There is no result guarantying the existence and unicity of the solution to the Cauchy problem represented by governing equations of the conceptual model and any complete set of initial conditions. Furthermore, the theoretical attempts to prove the existence of the a weak solution for the Riemann problem fail because of the source terms, namely friction and non-equilibrium sediment transport. Fraccarollo and Capart (2002) attempted to show that there is a time window where the effects of flow friction are negligible and were local equilibrium is a valid hypothesis for the sediment transport. Although the results of Fraccarollo and Capart (2002) are strictly valid for erosional flows and for a particular conception of a frictional time scale, it will be assumed that

there is indeed a time window for which geomorphic dam-break flows feature equilibrium sediment transport and are marginally affected by the bed shear stress. The conservation equations become homogeneous and are susceptible to be written in the following quasi-conservative form

$$\partial_t (h + Y_b) + \partial_x (hu) = 0 \tag{2}$$

$$\partial_t (a_m hu) + \partial_x \left(a_c u_c^2 h_c + u_s^2 h_s + g\left(\tfrac{1}{2}h_s^2 + \tfrac{1}{2}a_c h_c^2 + h_s h_c\right)\right) + g(a_c h_c + h_s)\,\partial_x (Y_b) = 0 \tag{3}$$

$$\partial_t ((1-p)Y_b + C_c h_c) + \partial_x (Chu) = 0 \tag{4}$$

where h is the water depth, u is the depth averaged flow velocity, Y_b is the bed elevation, h_c, u_c and C_c are, respectively, the thickness, the depthaveraged velocity and the flux-averaged concentration of the contact load layer, h_s and u_s are, respectively, the thickness and the depth-averaged velocity of the suspended sediment layer, $a_m = 1 + (s-1)C$, $a_c = 1 + (s-1)C_c$, s is the specific gravity of the sediments, C is the flow-averaged sediment concentration and g is the acceleration of gravity. The concentration C_s was eliminated since its value is generally much lower than C_c.

Equations (2) to (4) can be solved for the total flow depth, h, the layer-averaged flow velocity, u, and the bed elevation, Y_b. Closure equations for C_c and h_c are derived from the dynamics of the contact load layer (details *in* Ferreira 2005, pp. 277–289). They read

$$C_c = \frac{\theta d_s}{tan(\varphi_b) h_c} \tag{5}$$

$$h_c = m_1 \theta + m_2 \tag{6}$$

The variables and parameters in equations (5) and (6) are θ, the Shields parameter, defined as $\theta = C_f u^2/(g(s-1)d_s)$, d_s the particle diameter, $tan(\varphi_b)$, the ratio of shear to normal stresses near the bed and m_1 and m_2, parameters that should depend on the mechanical properties of the sediment particles, on its diameter and density and on the viscosity of the fluid. Ferreira (2005), pp. 283–285, hypothesized that, for a given fluid, m_1 and m_2 may show little variation with the particle properties and can be considered constants. In this work, it is considered that $m_1 = 6.5$ and $m_2 = 1.5$. The depth-averaged velocity in the contact layer is obtained assuming that $u(y)/u_* \propto (y/h_c)^{\frac{1}{6}}$ where $u_*^2 = C_f u^2$ is the friction velocity. Depth-averaging over the layer thickness, it is obtained

$$u_c = u \left(\frac{h_c}{h}\right)^{\frac{1}{6}} \tag{7}$$

Although equations (2) to (4) express the conservation of fundamental flow quantities and despite being homogeneous equations, Glimm's theorem Glimm (1965) for the existence and unicity of weak solutions of the Riemann problem can not be directly applied. This is so because equations (2) to (4) cannot be written in pure conservative form. Indeed, term $g(a_c h_c + h_s)\partial_x(Y_b)$ represents a source of momentum and is not reducible to a conservative flux.

Ferreira (2005), pp. 361–363, using Glimm's theorem, attempted to prove the existence of weak solutions for the Riemann problem

$$\partial_t (\mathbf{V}(\mathbf{U})) + \partial_x (\mathbf{F}(\mathbf{U})) + \mathsf{A}\partial_x (\mathbf{V}(\mathbf{U})) = \mathbf{G}(\mathbf{U}) \tag{8}$$

$$\mathbf{U}_0 \equiv \mathbf{U}(x, t=0) = \begin{cases} \mathbf{U}_\mathrm{L} & \text{if } x < 0 \\ \mathbf{U}_\mathrm{R} & \text{if } x \geq 0 \end{cases} \tag{9}$$

where equation (8) condenses equations (2) to (4) and where A is a matrix such that $\mathsf{A}_{23} = g(a_c h_c + h_s)$ and $\mathsf{A}_{ij} = 0, (i,j) \neq (2,\ 3)$. Weak solutions were shown to exist but they are not unique. In fact, existence can only be asserted if A is linearized across discontinuities. Thus, the solution depends on the specific linearization carried out. The Rankine-Hugoniot jump conditions derived from the integral form of equation (8) become

$$(\mathbf{U}_\mathrm{d} - \mathbf{U}_\mathrm{u})\, S_j = (\mathbf{F}_\mathrm{d} - \mathbf{F}_\mathrm{u}) + \mathsf{A}^* (\mathbf{U}_\mathrm{d} - \mathbf{U}_\mathrm{u}) \tag{10}$$

where S_j is the velocity of the shock associated to the $\lambda^{(j)}$-characteristic field, A^* is the linearized matrix A and d and the subscripts u stand for "downstream" and "upstream", respectively. A consistent linearization can be obtained by averaging the terms across the discontinuity.

Ferreira (2005), pp. 363–366, showed that the weak solution of system (8) subjected to (9), in which $\mathbf{U}_0$ expresses the geometry seen in Figure 1, admits two types of self-similar solutions, depending on the values of h_L, Y_{b_L} and h_R. If the eigenvalues associated to the eigenvectors of system (8) are such that $\lambda^{(1)} > \lambda^{(2)} > \lambda^{(3)}$, the solution of type A comprises one expansion wave associated to the $\lambda^{(3)}$-characteristic field initial and two shock waves, associated to the $\lambda^{(2)}$- and the $\lambda^{(1)}$-characteristic fields. The wave structure of each of these solutions, represented in the x–t plane, can be seen in Figure 2. The corresponding flow profiles are shown in Figure 3. Solution of type B, first studied by Fraccarollo and Capart (2002) in the wake of Fraccarollo and Armanini (1999), does not admit 2-jumps. On the contrary, in the solution of type A, the shock associated to $\lambda^{(2)}$ is a flow feature that may be associated to the 2-jump.

It is noted that the $\lambda^{(2)}$-shock features a negative jump in the flow depth and a positive, aggradational, jump in the bed elevation. The direction of propagation and the type of morphological impacts featured by the observed jump provide the fundamental criteria to decide whether it is a flow structure describable by a

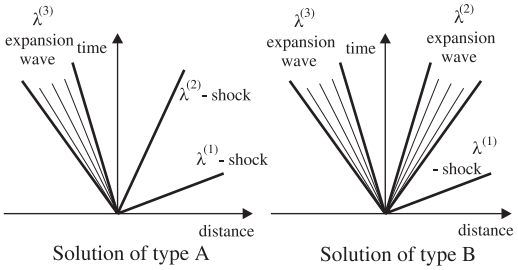

Figure 2. Wave structure of the weak solution of the Riemann problem constituted by system (8) subjected to the initial conditions (9). Left: solution of type A; right: solution of type B.

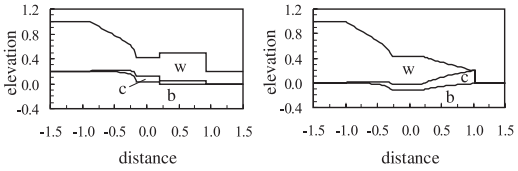

Figure 3. Flow profiles corresponding to the weak solution of the Riemann problem constituted by system (8) subjected to the initial conditions (9). Left: solution of type A; right: solution of type B. The flow regions are: w – clear water/suspended sediment layer; c – contact load layer and b – bed.

Riemann shock or one that requires different conceptualization. Thus, 2-jumps that migrate upstream and that are associated to scour in the bed are clearly not described by the flow and sediment dynamics included in equations (2) to (4).

3 EXPERIMENTAL PROCEDURES AND RESULTS

The experimental work took place in the laboratory of hydraulics of the Department of Civil and Environmental Engineering of the Université catholique de Louvain, Louvain-la-Neuve, Belgium. The experimental tests were performed in 6 m long and 25.1 cm wide horizontal channel. The dam was simulated by a vertical gate, placed at 3 m from the extremities, whose movement is directed downwards (Spinewine 2005, p. 56). A manually activated trigger releases the pressure of 7 bar, generated in a compressor, required to open the gate at a speed of about 5 m s^{-1}. The maximum non-dimensional time necessary to open the gate is $t_0^* = t_0\sqrt{\frac{9.8}{max(h_L)}} = 0.4$ where to is the maximum time necessary to open the gate and $max(h_L)$ is the maximum initial water depth behind the gate.

The experimental texts were recorded in digital video by a CCD camera acquiring 200 fps with the resolution of 512 × 1024. The flow was fully recorded in the downstream reach of the channel. Upstream the gate, only the first 0.8 m were recorded. Since the recording area is about 0.8 m wide per 0.5 m height, each test had to be repeated five times. In order to synchronise the runs, a TTL flash light visible by the camera in each of its positions is triggered by the gate release. It should be mentioned that the repeatability of the tests was found to be highly satisfactory provided that the sameness of the initial conditions was ensured with some zeal. A mote detailed description of the experimental set-up and of the tests, along with additional tests performed for other initial conditions and bed material, may be found in Spinewine (2005).

The sediment particles used in scale laboratory models seldom abide to the global geometric scale. As a result, the mobility of the sediment is generally underestimated. In order to increase sediment mobility, the tests were performed with PVC pellets with $s = 1.56\,\mathrm{kg\,m^{-3}}$. The equivalent diameter of a PVC particle – the diameter of a sphere with the same volume – is 3.9 mm. The dimensions of the particles exhibited little variability.

All tests featured a piecewise horizontal bed. In accordance with figure 1, the datum was set to the level of the downstream bed. It is important to note that the downstream bed was saturated in all tests, even if $h_R = 0$.

The fundamental non-dimensional parameters that describe the initial conditions illustrated in figure 1 must take into account the flow depth downstream the dam and the jump in the bed elevation across the dam. The particular choice of parameters employed in this text are

$$\alpha \equiv \frac{h_R + |min\,(0, Y_{b_L})|}{h_L + max\,(0, Y_{b_L})} \tag{11}$$

and

$$\delta \equiv \frac{Y_{b_L}}{h_L + max\,(0, Y_{b_L})} \tag{12}$$

The length scale implicit in (11) and (12) is

$$L_* = h_L + max\,(0, Y_{b_L})$$

From this length scale, time and velocity scales can be derived. It is obtained $T_* = \sqrt{\frac{L_*}{g}}$ and $U_* = \sqrt{gL_*}$, respectively.

The initial conditions for the nine experimental tests shown here, described with the variables presented in figure 1, are shown in Table 1.

The raw data obtained from the tests is composed of video footages taken in the five locations along the channel. This data was treated to render flow profiles (details in Amaral 2004). In this profiles three surfaces were identified: a) the free surface, b) the boundary between the transport layer and the clear water layer

Table 1. Summary of the initial data for experimental tests.

Name	h_L (m)	Y_{b_L} (m)	h_R (m)	L_* (m)	α (–)	δ (–)
25_-05_00	0.30	−0.05	0.00	0.30	0.167	−0.167
35_-05_00	0.40	−0.05	0.00	0.40	0.125	−0.125
25_00_00	0.25	0.00	0.00	0.25	0.000	0.000
35_00_00	0.35	0.00	0.00	0.35	0.000	0.000
35_05_00	0.30	0.05	0.00	0.35	0.000	0.143
25_05_00	0.20	0.05	0.00	0.25	0.000	0.200
35_10_00	0.25	0.10	0.00	0.35	0.000	0.286
25_05_05	0.20	0.05	0.05	0.25	0.200	0.200
35_10_10	0.25	0.10	0.10	0.35	0.286	0.286

and c) the boundary between the bed and the transport layer. The profile of the water depth was computed as the difference between the the free surface and the bed. From the water depth profiles, it was possible to estimate the location and the strength of the observed discontinuities at each instant.

4 COMPARISON BETWEEN EXPERIMENTAL AND THEORETICAL RESULTS

The observed flow profiles are shown in figure 4 – solution of type B – and 5 – solution of type A. The theoretical profiles, calculated from the weak solution of system (8) given the initial conditions discriminated in table 1, are also shown in these figures, superimposed to the flow profiles.

The values of the friction coefficient employed in the closure equations (5) and (6) are shown in Table 2. They were chosen so to achieve best agreement between the experimental and the theoretical profiles. Sediment concentrations are controlled by the value of $tan(\varphi_b)$. Lacking universally acknowledged estimates for this parameter, it was imposed $tan(\varphi_b) = 0.45$, a value chosen so that the maximum concentration in the contact load layer would be around 0.3 in all tests whose solution is of type B.

Both the experimental profiles and the theoretical solutions are shown in self-similar co-ordinates. It is observed that the thickness of the contact load layer and the minimum bed elevation are correctly estimated in almost all tests. Naturally, phenomena pertaining to soil mechanics, namely slope stability and *en masse* bed movement, could not have been reproduced by the theoretical solution since the governing equations do not incorporate formulations for those phenomena. Hence, the the steep slopes featured by the weak solutions at the end of the expansion wave associated to the $\lambda^{(3)}$– characteristic field in figures 4e, f and g are in clear contrast with the much gentler slopes featured by the observed profiles. This gentle slope was essentially formed at the beginning of the times when the gate was lowered: the sharp bed step could not be maintained by the cohesionless bed material; a fracture surface was formed at the toe of the step with the inclination of the rest angle of the particles; finally the sediment above this fracture surface entered the contact load layer and was eventually deposited further downstream. A simple mechanism accounting for this mass failure was proposed and tested by Spinewine and Zech (2005).

In the tests with a negative bed step (4a and b) the theoretical solution captures the bed profile reasonably well. It is observed that a steep positive slope results from the initial discontinuity. Presumably, it is the flow that provides the extra shear force tomaintain the bed slope larger than the submerged rest slope.

The instability of the initial bed step in the experimental texts shown in figure 5 obeyed same same mechanisms already explained for the tests depicted in figures 4e, f and g. However, because of the presence of a layer of water downstream, the transport capacity is much lower and the flow does not evolve into a debris-flow-like wave front. Hence, the bed material resulting from the initial bed step failure is deposited almost instantaneously at the toe of the step and, as the flow looses memory of the gatemovement, becomes a bed discontinuity progressing downstream along with the jump in water surface. As a result, the bed profile calculated along the expansion wave associated to the $\lambda^{(3)}$-characteristic field is, in these tests, a better description of the observed profile.

The effect of flow resistance is perceived in the observed profiles inasmuch they are not truly selfsimilar. This is particularly true for the flows depicted in figures 4. Furthermore, it is noticed that Froude similarity does not completely determine the flow profiles. If that was the case, parameters α and δ would suffice to determine the profiles. Instead, it is observed in figures 4c and d, whose profiles are both characterized by $\alpha = 0$ and $\delta = 0$, that neither the velocity of the wave front nor the overall shape of the profile is the same for both flows. Ferreira et al. (2006) propose that the shape of the self-similar profile of any flow variable U_i can, under certain simplifying conditions, be determined by

$$\Gamma_i = \Pi_i \left(\alpha, \delta, s, tan(\varphi_b), \frac{d_s}{L_*} \right) \tag{13}$$

In the present case, s and $tan(\varphi_b)$ are constants. Thus, the relative submersion of the particles, d_s/L_*, must be accounted for the differences in the observed profiles. The only way to introduce this effect in the theoretical solution is by varying the friction coefficient. This justifies the values of C_f seen in table 2.

Evidently, all flows exhibit a discontinuous wave front. As for the 2-jumps, their existence and the variables that characterize them were determined in accordance to the principles explained in section 3. It is clear that tests 25_-05_00, 35_-05_00 and 35_00_00

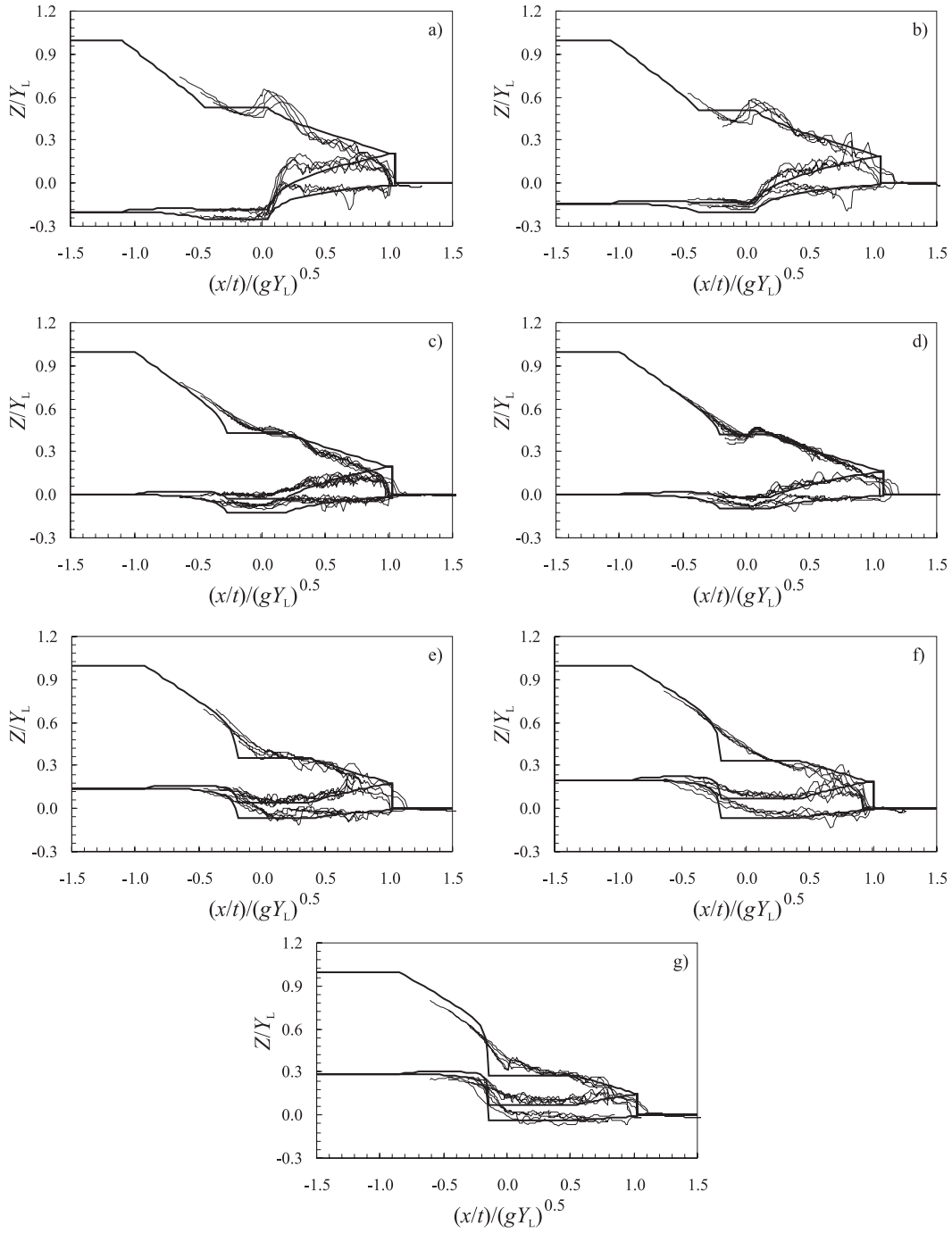

Figure 4. Flow profiles. Solution of type B. Profiles correspond to tests a) 25_-05_00; b) 35_-05_00; c) 25_00_00; d) 35_00_00; e) 35_05_00; f) 25_05_00; g) 35_10_00. Solid thick lines (———) stand for the theoretical solution while solid thin lines (———) stand for the observed profiles.

Table 2. Friction coefficient employed in equations (5) and (6).

Name	α (–)	δ (–)	C_f (–)
25_-05_00	0.167	−0.167	0.017
35_-05_00	0.125	−0.125	0.015
25_00_00	0.000	0.000	0.017
35_00_00	0.000	0.000	0.012
35_05_00	0.000	0.143	0.015
25_05_00	0.000	0.200	0.017
35_10_00	0.000	0.286	0.012
25_05_05	0.200	0.200	0.012
35_10_10	0.286	0.286	0.012

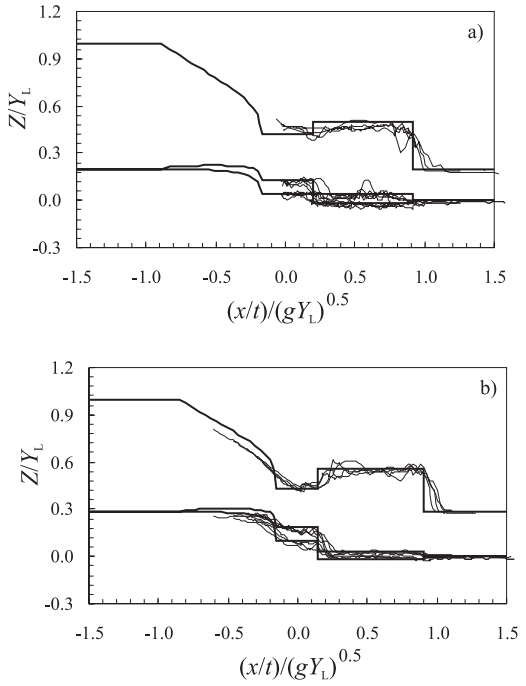

Figure 5. Flow profiles. Solution of type A. Profiles correspond to a) 25_05_05; b) 35_10_10. Solid thick lines (———) stand for the theoretical solution while solid thin lines (——) stand for the observed profiles.

(figure 4a, b and d) develop 2-jumps that progress upstream. Tests 25_05_05 and 35_10_10 (figures 5a and b) develop 2-jumps that move downstream. The properties of these discontinuities will be discussed in the next section.

5 DISCUSSION

In both solutions, the shock associated to the $\lambda^{(1)}$-characteristic field is physically identifiable with the wave-front (see figures 4 and 5). On the contrary, the 2-jump may not always be identifiable by the shock associated to the $\lambda^{(2)}$-characteristic field in the solution of type A. Indeed, it is clear from figures 2 (left) and 5 that this is a downstream progressing shock, while the observed 2-jumps often migrate upstream.

The dynamics and the kinematics of the wavefront are sufficiently well described by the Rankine-Hugoniot jump conditions, equations (10) with $j = 1$. Indeed, the strength of the wavefront, defined as $h_R - h_1$, remains approximately constant throughout the duration of the experimental test (see figure **??**) which enables a meaningful comparison between the weak solutions and the experimental profiles.

The velocity of the wavefront, however, decreases over time, as seen in figure 6, especially for the tests for which $h_R = 0$ (figures 6a to f). This fact prompted Leal et al. (2006) to describe the path of the wavefront in the x_t plane as a 2nd order equation. There is no appreciable decrease in the velocity of the wavefront in the experiments for which $h_R > 0$. This suggests that bottom friction is the main responsible for the delay of the wavefront.

Since bottom friction is not included in the weak solution of 8, in order to delay the velocity of the wavefront in the theoretical solution it is necessary to increase the factors that affect S_1 in 10. Such factors are related to the inertia of the contact load layer and are expressed by its thickness and the sediment concentration. Given that $tan(\varphi_b)$, m_1 and m_2 are constants, a good agreement of the observed and the calculated wavefront velocity requires a good estimate for the friction coefficient C_f.

The influence of d_s/L_* can only be addressed in the theoretical solution with adjustments of the friction factor. Thus, the correct modeling of the velocity of the wavefronts of tests 25_00_00 ($d_s/L_* = 0.0180$) and 35_00_00 ($d_s/L_* = 0.0129$), both characterized by $\alpha = 0$ and $\delta = 0$ can only be attained if the friction factor relative to 25_00_00 is increased. Indeed, as seen in figure 6c, the non-dimensional velocity of the wavefront of the test characterized by $d_s/L_* = 0.0180$ is smaller than that of the test for which $d_s/L_* = 0.0129$. As expected, the friction coefficient is larger for the flow with the smaller relative submersion.

An undesirable consequence of the increase of C_f is the increase of the flow depth in the first constant state (the state upstream the $\lambda^{(2)}$-shock). As seen in figure 7, the theoretical shock strength is consistently overestimated, for the same initial conditions.

Fraccarollo and Capart (2002) noticed that the wavefront propagates as an erosional shock. Since it is associated to the $\lambda^{(1)}$-characteristic field, it is fundamentally a hydrodynamically-driven shock: the bed jump is comparatively small. On the contrary, Ferreira 2005, §5.2.2, showed that the $\lambda^{(2)}$-shock is always an aggradational shock in which morphodynamics is of

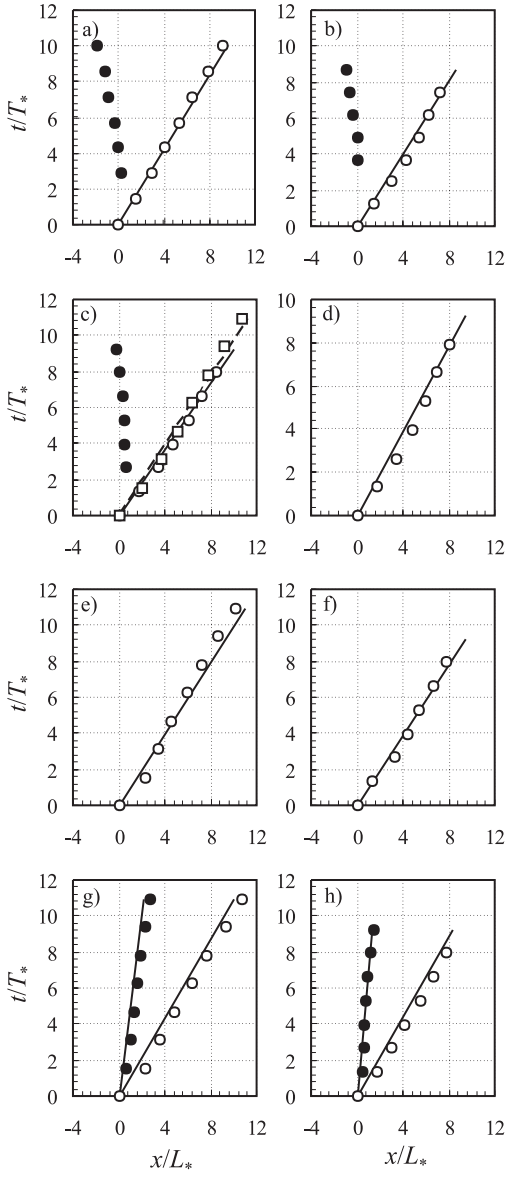

Figure 6. Calculated and measured non-dimensional shock paths. a) $\alpha = 0.167$, $\delta = -0.167$; b) $\alpha = 0.125$, $\delta = -0.125$; c) $\alpha = 0.0$, $\delta = 0.0$ (features tests with $d_s/L_* = 0.0129$ and $d_s/L_* = 0.0180$); d) $\alpha = 0.0$, $\delta = 0.143$; e) $\alpha = 0.0$, $\delta = 0.200$; f) $\alpha = 0.0$, $\delta = 0.286$; g) $\alpha = 0.200$, $\delta = 0.200$; h) $\alpha = 0.286$, $\delta = 0.286$. Solid lines (——) stand for the calculated path of the $\lambda^{(1)}$-and the $\lambda^{(2)}$-shocks; open circles (○) stand for the measured path of wavefront; solid circles (●) stand for the measured path of the 2-jump. In figure c), the convention is maintained for the test with $d_s/L_* = 0.0129$; for the test with $d_s/L_* = 0.0180$, the dashed line (- - - -) stands for the calculated path of the $\lambda^{(1)}$-shock and the open squares (□) stand for the measured path of the wavefront.

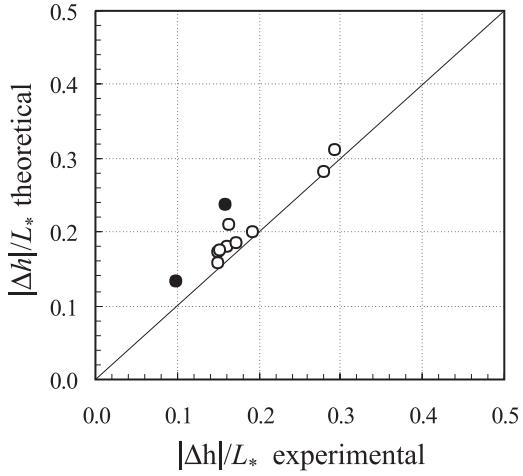

Figure 7. Calculated and measured non-dimensional shock strengths in terms of flow depths. Open circles (○) stand for the wavefront; solid circles (●) stand for the 2-jump.

paramount importance. Since the influence of the variables that describe sediment dynamics is strong in the $\lambda^{(2)}$-characteristic field, the dynamics of the associated shock are fundamentally determined by the solid phase: the $\lambda^{(2)}$-shock progresses with the velocity of propagation of the jump in the bed, much slower than the wavefront.

The experimental work revealed that only the tests depicted in figure 5 featured 2-jumps susceptible to be identified with the $\lambda^{(2)}$-shock. These downstream-progressing discontinuities are driven by the dunelike advancement of a sharp-edged bed wave. The strong coupling between hydrodynamic and morphodynamic variables in the $\lambda^{(2)}$-characteristic field is revealed by the fact that the strength of the shock is of the same magnitude in both types of variables.

Because of the correct coupling between hydrodynamic and morphodynamic variables, the results of the weak solution are a good reproduction of the observed behavior, especially in what concerns the shock velocity (see 6g and h). The shock strength is less well reproduced. As seen in figure 7, the shock strength is overestimated by the theoretical solution. This is mainly due to the fact that the weak solution overestimates the bed elevation in the 2nd constant state.

It is proposed that 2-jumps that occur in geomorphic dam-break flows whose mathematical description is a weak solution of type A are well described by the $\lambda^{(2)}$-shock. Its dynamics traduce the equilibrium of the flux and inertial terms across the shock, being the gravity-related term included in the flux terms, once linearized in accordance with equation 10.

Other types of 2-jump were found in the experimental tests whose profiles are depicted in figures 4. The mathematical description of these tests is a weak solution of type B. Ferreira et al. (2006) determined the locus, in the α–δ plane, of the boundary between solutions of types A and B. When $\alpha = 0$ the solution is necessarily of type B. If $\alpha > 0$ and $\delta < 0$, the solution is also of type B. It follows from the fact that type B solutions exhibit a continuous wave associated to the $\lambda^{(2)}$-characteristic field, that any 2-jump developing from such initial conditions can not be described by the jump conditions (10).

Alcrudo and Benkhaldoun (2001) developed a theoretical solution for the dam-break flow over fixed bed with a discontinuity in the dam location. Their solution features an extra discontinuity, a jump born in the source term that describes the force of gravity. Such discontinuity is impossible in mobile bed problems, as the derivative of the bed elevation, $\partial_x(Y_b)$, ceases to be treated as a source. Thus, the origin of these 2-jumps must be searched in interaction between the bed and the flow in the first instants.

It is observed that these 2-jumps are associated with important scour at the vicinity of the dam. Capart and Young (1998), working with almost neutrally buoyant particles ($s = 1.05$), observed a 2-jump with these properties and whose upstream velocity is comparable to those shown in figures 6a, b and d. They proposed that bottom friction could be a cause of the jump, by slowing down the wavefront.Mathematically, the characteristics in the $\lambda^{(2)}$-characteristic field would fold backwards in the x–t plane until converging into a compressive shock. Capart and Young (1998) backed these model with the early studies of Dressler (1954) on the influence of bottom friction. Numerical experiments carried out for fixed and mobile beds Ferreira et al. (2006) have shown that it is always possible to find continuous solutions even in the presence of very large bottom friction. It is thus unlikely that this 2-jump is mainly originated by the compressing of the $\lambda^{(2)}$-characteristic field under the effect of friction.

Chen and Simons (1979) report an upstream progressing 2-jump in a bed featuring an initial positive bed step. Chen and Simons (1979) believe that the jump is originated by the increased flow velocity over the bed discontinuity, as it would occur in a weir. Although their initial conditions are difficult to interpret, their results may be used to state the case for the influence of two-dimensional effects in the first stages of the flow. A highly accelerated parcel of flow directed downwards would originate an scour hole, not explainable by the shallow water theory. Once formed, this accelerated flow region would progress upstream, a process similar to the knickpoint migration. This would explain the 2-jump observed in test 35_00_00 (figure 4d).

The jumps seen in the tests featuring an initial negative bed step, 25_-05_00 and 35_-05_00 (figures 4a and b) may also owe to two-dimensional flow effects. An accelerated parcel of flow directed upwards would be susceptible to slow down the flow in the vicinity of the bed jump, thus provoking the free surface elevation seen in figures 4a and b. The hydrodynamic response to compatibilize the supercritical and subcritical flow regimes thus created would be forming a jump. It would progress upstream in an antidune-like movement.

6 CONCLUSION

The present study attempted to contribute to the characterization of the discontinuities observed in geomorphic dam-break flows. Special attention was conceded to the often observed 2-jump that forms at early times at the location of the dam.

A comparison between experimental flow profiles and the weak solution of the dam-break Riemann revealed that there is a class of 2-jumps whose mechanics are susceptible to be described by the Rankine-Hugoniot conditions of the shock associated to the $\lambda^{(2)}$-characteristic field. The distinctive traits of these 2-jumps are its positive velocity of propagation and, in what concerns bed morphology, its aggradational nature.

When the weak solution features an expansion wave in the $\lambda^{(2)}$-characteristic field, the causes of the 2-jump must be searched outside the realm of phenomena described by the homogeneous onedimensional governing equations. It is observed that these 2-jumps migrate upstream and are associated to scour holes. Possible explanations comprise: i) frictional effects combined with non-equilibrium sediment transport and; ii) two-dimensional flow effects. More likely, a combination of the preceding effects may be the cause of these 2-jumps. Hence, this flow features certainly call for more effort in their empirical characterization.

ACKNOWLEDGEMENTS

The authors acknowledge the financial support granted by the European Commission to the project IMPACT, under the 5th framework (1998-2002), thematic program for Environment and Sustainable development, officiated by Karen Fabbri.

REFERENCES

Alcrudo, F. and F. Benkhaldoun (2001). Exact solutions to the riemann problem of the shallow water equations with a bottom step. *Computers & Fluids 30*, 643–671.

Amaral, S. R. C. (2004). *Experimental Characterization of 1-D Dam-Break Waves over Cohesionless Sediment Beds*. Final Project for the Graduation in Civil Engineering. Instituto Superior Técnico, Technical University of Lisbon.

Capart, H. (2000). *Dam-break induced geomorphic flows and the transition from solid- to fluid-like behaviour across evolving interfaces.* Ph.D. thesis, Université catholique de Louvain, Louvain-la-Neuve, Belgium.

Capart, H. and D. L. Young (1998). Formation of a jump by the dam-break wave over a granular bed. *J. Fluid Mech. 372*, 165–187.

Chapman, S. and T. G. Cowling (1970). *The Mathematical Theory of Non-Uniform Gases* (3rd ed.). Cambridge, UK: Cambridge University Press.

Chen, Y. H. and D. B. Simons (1979). An experimental study of hydraulic and geomorphic changes in an alluvial channel induced by failure of a dam. *Water Resour. Res. 15*(5), 1183–1188.

Dressler, R. F. (1954). Comparison of theories and experiments for the hydraulic dambreak wave. In *Assemblée General de Rome*, Volume 3, pp. 319–328. Intl. Assoc. of Hydrology.

Ferreira, R. M. L. (2005). *River Morphodynamics and Sediment Transport. Conceptual model and solutions.* Ph.D. thesis, Instituto Superior Técnico, Technical University of Lisbon, Lisboa, Portugal.

Ferreira, R. M. L., J. G. A. B. Leal, A. H. Cardoso, and A. B. de Almeida (2003). Sediment transport by dam-break flows. a conceptual framework drawn from the theories for rapid granular flows. In *Proc. of the 3rd IMPACT Workshop*, Louvain-la-Neuve, Belgium (edited in CD-ROM).

Ferreira, R. M. L., J. G. B. Leal, and A. H. Cardoso (2006). Sensitivity analysis of a riemann solution for the shallow-water equations. *in preparation*.

Fraccarollo, L. and A. Armanini (1999). A semianalytical solution for the dam-break problem over a mobile bed. In *Proc. of 1st IAHR Symposium of River, Coastal and Estuarine Morphodynamics (RCEM)*, Volume 1, pp. 361–369. University of Genova, Genova, Italy.

Fraccarollo, L. and H. Capart (2002). Riemann wave description of erosional dam-break flows. *J. Fluid Mech. 461*, 183–228.

Glimm, J. (1965). Solutions in the large for nonlinear hyperbolic systems of equations. *Comm. Pure Appl. Math. 18*, 697–715.

Leal, J. G. A. B., R. M. L. Ferreira, and A. H. Cardoso (2002). Dam-break waves on movable bed. In D. Bousmar and Y. Zech (Eds.), *RIVER FLOW 2002*, Volume 2, pp. 981–990. Balkema.

Leal, J. G. A. B., R.M. L. Ferreira, and A. H. Cardoso (2006). Dam break wave front celerity. *J. Hydraul. Eng. 132*(1), 69–76.

Spinewine, B. (2005). *Two-layer flow behaviour and the effects of granular dilatancy in dambreak induced sheet-flow*. Ph.D. thesis, Université catholique de Louvain, Louvain-la-Neuve, Belgium.

Spinewine, B. and Y. Zech (2005). Dam-break on a movable bed in presence of an initial bed discontinuity: laboratory experiments and simulations with a multi-layer shallow water model. In *Proc. of XXXI IAHR Congress, Theme D*, Seoul, South Korea, pp. 3434–3445.

Stoker, J. J. (1958). *Water Waves. The Mathematical theory with applications*. Wiley-Interscience Publication (reprinted in 1992).

Zech, Y., S. S. Frazão, B. S. ans Nicholas Le Grelle, A. Armanini, L. Fraccarollo, M. Larcher, R. Fabrizi, M. Giuliani, A. Paquier, K. El Kadi, R. M. L. Ferreira, J. G. A. B. Leal, A. H. Cardoso, and A. B. de Almeida (2004). Sediment movement model development. In *Proc. of Dam Safety 2004, ASDSO National Conference*, Volume 2, Phoenix, USA. Association of State Dam Safety Officials (ed. CD-ROM).